remote sensing

MDPI

Technical Note

Data Fusion for Satellite-Derived Earth Surface: The 2021 Topographic Map of Etna Volcano

Gaetana Ganci *, Annalisa Cappello and Marco Neri

Istituto Nazionale di Geofisica e Vulcanologia, Osservatorio Etneo-Sezione di Catania, 95125 Catania, Italy
* Correspondence: gaetana.ganci@ingv.it

Abstract: We present a new automatic procedure for updating digital topographic data from multi-source satellite imagery, which consists in the production of Digital Surface Models (DSMs) from high resolution optical satellite images, followed by a context-aware fusion that exploits the complementary characteristics of the multi-source DSMs. The fused DSM minimizes blunders and artifacts due to occlusions (e.g., the presence of clouds, snow or ash plumes) in the source images, resulting in improved accuracy and quality versus those that are not merged. The procedure has been tested to produce the 2021 digital topography of Mt Etna, whose summit area is constantly changing and shows the new peak of 3347 m on the north rim of the South East Crater. We also employ the 2021 DSM to measure the volcanic deposits emplaced in the last five years, finding about 120 million cubic meters, with a yearly average volume of about 24 million cubic meters in agreement with the large eruptive rates registered at Mt Etna since the nineteen seventies. The flexibility and modularity of the presented procedure make it easily exportable to other environmental contexts, allowing for a fast and frequent reconstruction of topographic surfaces even in extreme environments.

Keywords: Digital Surface Models; data fusion; optical satellite imagery; morphological changes; Etna

Citation: Ganci, G.; Cappello, A.; Neri, M. Data Fusion for Satellite-Derived Earth Surface: The 2021 Topographic Map of Etna Volcano. *Remote Sens.* **2023**, *15*, 198. https://doi.org/10.3390/rs15010198

Academic Editor: Balázs Székely

Received: 9 November 2022
Revised: 19 December 2022
Accepted: 22 December 2022
Published: 30 December 2022

1. Introduction

Observing and measuring morphological changes at the surface of an active volcano is of paramount importance to understand the processes that cause both growth and erosion of landforms and to evaluate and forecast the related hazards [1]. The building of updated Digital Surface Models (DSMs) and comparison with previous models are unique means of assessing rapid topographic variations, the volume of lava erupted or the rate of dome growth at an active volcano [2–5], monitor the dynamic evolution of glaciers [6], measure debris flow thickness [7], and understand sediment transport in a river or stream bed [8]. Moreover, accurate and updated DSMs are fundamental input to obtain reliable results when simulating geophysical flows such as lava flows, pyroclastic flows, debris avalanches and lahars, and to assess the volcanic hazard and risk (see e.g., [9–11]).

A DSM is a representation of the topographic surface of the Earth that includes the natural and built environment. DSMs are generally derived from three main sources: (i) Ground surveys, which is the most traditional technique, consisting in the accurate field measurement of point elevations; (ii) Hardcopy topographic maps, used as base maps to derive e.g., digital contour lines, elevation points and hydrographic features; (iii) Remote sensing, based on the processing of imagery acquired from airborne or satellite platforms, such as photogrammetry, laser or radar. All these data sources require different processing methods and provide different areal coverages, with variable levels of spatial accuracy and detail, as well as of temporal frequency.

Among these techniques, satellite remote sensing is becoming more and more popular since it can be effective and efficient [12]. Two primary methods for generating digital elevation data are: (i) photogrammetry techniques using visible and infrared imagery, or radar data (radargrammetry), and (ii) radar interferometry (see e.g., [13,14]).

In extreme environments, such as the summit areas of active volcanoes, which are often impractical due to the continuous morphological instability deriving from the volcanic activity itself, as well as due to the strong winds and continuous gas emissions, radar data are difficult to process because of the lack of coherence between images. Moreover, summit areas are often affected by the presence of snow during the winter and sometimes permanent glaciers. Common phenomena that cause moderate thickness deposits are linked to local transport and erosion due to the accumulation of snow in the colder seasons and the following melting in spring [15]. A further aspect to take into consideration is the fact that human activities, such as earthworks for the construction of driveways or simple tourist paths, can greatly contribute to significantly modify topographic surfaces, albeit in limited areas; this is demonstrated, for example, by the continuous trampling along the paths mostly used by hikers on Etna (up to many tens of thousands per year), as documented by [16] for the surfaces located on the rim of the 2002–2003 pyroclastic cones, which in those points, a few years after their genesis, was about 2 m lower. On the other hand, photogrammetry applied to optical satellite imagery is becoming a preferred way to gather topographic information, since a multitude of new sensors, able to acquire very-high-resolution optical data in stereo or tristereo, provides an abundance of source data to quickly observe large areas [17]. Furthermore, there is a tendency in the recent matching algorithms to prefer temporally close acquisitions, common in recent stereo or tristereo acquisitions, showing the same visibility and atmospheric conditions, to the detriment of the base-to-height ratio in a way to increase the number of control points between the different images [18].

However, the products generated from satellite data can show several fictitious irregularities linked above all to the fact that the optical data are often affected by atmospheric conditions, in particular by cloud coverage, by the acquisition geometries and by the base-to-height ratio. In active open conduct volcanoes, such as Etna, obtaining optimal coverage is very difficult, besides the normal cloud coverage in the summit, due to the continuous summit degassing activity and the prevailing winds, which often impact the same areas. Finally, another major factor impacting the quality of DSMs derived by optical satellite images in volcanic areas is the presence of poor textured surfaces especially in the gentle slope or flat areas covered by volcanic sands [19].

The concurrent occurrence of these factors (clouds, volcanic degassing, slopes and rims crater morphological instability, snow cover, anthropogenic activities) and the continuous morpho-structural changes due to the eruptive activity make it very arduous to update the full three-dimensional model of an active volcano, especially when it is derived from just one stereo or tristereo acquisition. At the same time, it is required to develop new means to automatically process the abundance of data available.

To take advantage of the different DSM products in use today, researchers have resorted to fusion for deriving more comprehensive and enhanced digital elevation datasets that combine the complementary characteristics of source DSMs. Data fusion is the process of integrating data from multiple sources to improve consistency and accuracy than that provided by any individual data source [20]. Fusion techniques are useful for a variety of applications, including object recognition, identification and classification, change detection, object motion, etc. In remote sensing, data fusion has been used to integrate data acquired by different sensors mounted e.g., on satellites, aircraft and ground platforms, to produce more detailed and accurate fused products.

Here we present a new automatic procedure for DSM production and fusion in volcanic environments to capitalize on the available optical satellite images and obtain a merged DSM. The procedure consists in deriving single DSMs from different satellite imagery and fusing them to deliver a more complete, accurate and reliable elevation dataset that takes advantage of the complementary characteristics of the multi-source DSMs.

Our procedure has been applied here to obtain the 2021 DSM of Etna volcano, one of the most active volcanoes on Earth, whose top is subject to rapid morpho-structural changes, for which having accurate and updated topographic maps is crucial for hazard purposes.

2. Materials and Methods

We present a new simple and effective algorithm for fusing DSMs derived from optical satellite images with the main objective of improving the accuracy of the 3D reconstruction, minimizing the human bias in the fusion process. Input data consist of DSMs of the same target area, which can have different spatial resolutions or have been obtained from different satellite sensors. The processing steps characterizing the proposed algorithm, summarized in Figure 1, are:

1. Regridding and coregistration of the different DSMs;
2. Domain decompositions of the DSMs into patches;
3. Patches decomposition;
4. Selection of the best sub-patch;
5. Preliminary DSMs production;
6. Production of the final DSM.

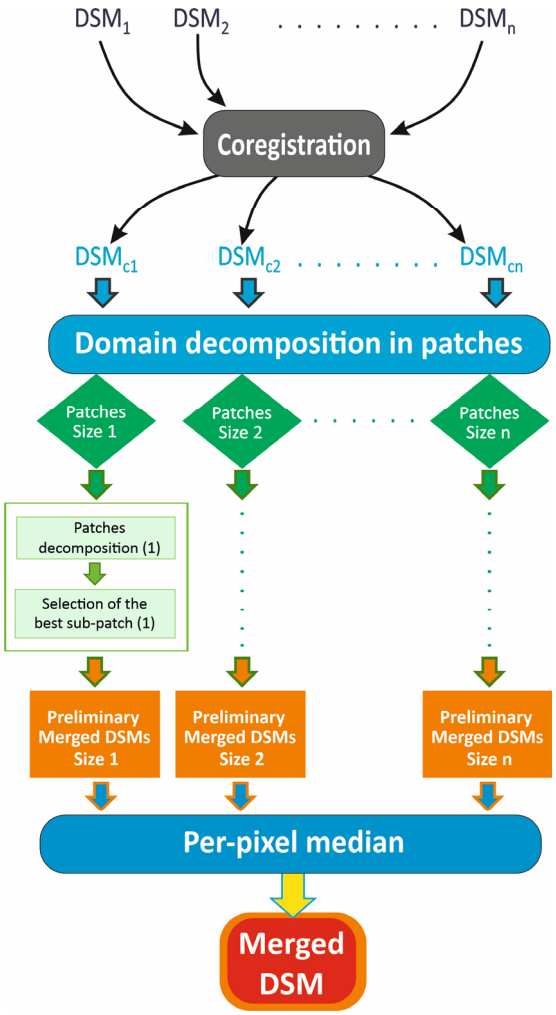

Figure 1. Scheme of the algorithm developed for Digital Surface Models (DSM) fusion. See text for explanation.

Regridding and Coregistration of the different DSMs

The first step includes mandatory preliminary processing operations and consists in resizing all DSMs in the same overlapping domain and exporting them in the same grid for the co-registration. Co-registration is accomplished through the Nuth and Kaab algorithm implemented in the dem_align python routine available on github [21]. After removing the horizontal mismatch, the DSMs are vertically aligned to a previous validated DSM. A

masking operation is also required for those areas subject to morphological changes in the period between the different acquisitions.

Domain decompositions of the DSMs into patches

All the DSMs are divided into regular sub-regions or patches. A minimum and a maximum size for the patch is established and different decompositions are accomplished for all the DSMs according to patch sizes. This domain decomposition serves to remove the scalability limitations and leads to optimal selection among the available information.

Patches decomposition

A second step of discretization is employed at patch level. Indeed, for each patch configuration, and for each square path, two different sub-regions are determined using a morphological filtering based on the slope, i.e., the slope median value of the patch is computed and used as threshold to divide the pixels of the patch into two groups that are separately treated. This step is required to take into account the geomorphological characteristics of the terrain in the attempt to avoid vertical errors due to at terrain with steep slopes.

Selection of the best sub-patch

For each patch size the best sub-patch among all the available decomposed DSMs is selected. In particular, the Laplace's differential operator ∇^2 is applied to the elevation function $\phi(x,y)$ of each point in a bidimensional space:

$$\nabla^2\varphi(x,y) = \frac{\partial^2\varphi}{\partial x^2} + \frac{\partial^2\varphi}{\partial y^2} \tag{1}$$

This operator can be discretized considering the value of elevation for each pixel $\varphi_{i,j}$ with respect to its Moore neighbors, by using spacing equal to 1:

$$L_{i,j} = \frac{\varphi_{i+1,j-1} + \varphi_{i+1,j} + \varphi_{i+1,j+1} + \varphi_{i,j-1} + \varphi_{i,j+1} + \varphi_{i-1,j-1} + \varphi_{i-1,j} + \varphi_{i-1,j+1}}{8} - \varphi_{i,j} \tag{2}$$

This operator, which is generally used in image processing to retrieve the edge of an image, enhances abrupt changes in the elevation due to clouds, plumes or other artifacts.

The standard deviation of the Laplacian operator is computed to evaluate the quality in each subregion for all the available DSMs.

Preliminary DSMs production

For each patch size, a preliminary DSM is produced mosaicing the best sub-patch obtained taking those with the minimum standard deviation of the Laplacian operator. In this way, for each subregion we assure the most regular DSM avoiding artifacts.

Production of the final DSM

Steps 4 and 5 are repeated for all the patch sizes considered, in this way a number of preliminary DSMs equal to the number of patch sizes is retrieved. The final merged DSM is obtained as the pixel-per-pixel median values of all the preliminary merged DSMs.

The presented algorithm is a cost-effective package that does not require high-performance computing resources. The result of this computation is a weighted average approach among a number of intermediate DSMs, with the weights automatically derived from the pixel per pixel median value. At the same time, taking into account the different size patches and their slopes, assures a homogeneous final product that minimizes blunders and artifacts. Moreover, this algorithm is not restricted to the fusion of two DSMs as most literature algorithms, but can be applied to as many DSMs as are available.

The 2021 Etna Summit Study Case

We tested our algorithm to update the topography of Mt Etna volcano. Today, four active craters are on the summit this volcano: Voragine (VOR, built in 1945) and Bocca Nuova (BN, 1968) are located inside the former Central Crater (1858); the North-East Crater (NEC) is a cinder cone that built up from 1911 (this crater represented the highest peak of Etna until 2020, i.e., 3320 m a.s.l.); the South-East Crater (SEC), formed during the 1971 eruption, has been the most active summit crater over recent decades. From 2016 to

today, VOR, BN and NEC have undergone striking morpho-structural transformations, alternating subsidence (up to hundreds of meters), intra-crateric Strombolian activity, lava fountaining and the growth of pyroclastic cones [22–24]. In the same period, the SEC was also very active, producing several dozens of intra-crateric lava fountains and lava flows from subterminal eruptive fissures opened on the slopes of the cone and at its base that expanded southward, between the 2002–2003 pyroclastic cones (Mts. Barbagallo) and Mt. Frumento Supino, and towards the East. In the second case, the lava flows were distributed along the western wall of the Valle del Bove and on the valley floor, reaching a maximum length of ~5–6 km [24,25]. Furthermore, on 24–27 December 2018 a flank eruption originated from a fissure located along the western wall of the Valle del Bove, producing a lava flow that traveled for about 3 km in length on the valley floor, also contributing to modify the morphology of the places [26,27].

The summit area experienced an unprecedented morphological variation particularly during 2021. Indeed, from January to July 2021, more than 50 eruptive events occurred at the SEC, which were characterized by the emission of sustained eruptive columns and lavas flows, combined with several collapses followed by pyroclastic avalanches [28].

The input to the fusion algorithm were three DSMs of July 2021 derived from two tristereo Pleiades acquisitions of 13 (Figure 2a) and 25 July 2021 (Figure 2c) and a stereo WorldView-1 acquisition of 27 July 2021 (Figure 2e), having a spatial resolution of 0.5 m. Along-track incidence angles of the three images are respectively −11.3°, 1.0°, and 11.2° and −14.1°, 4.8° and 10.3° for the forward (F), near-nadir (N), and backward (B) viewing geometries, while the across-track angle varies between −2° and 3° and between −3.9° and −5.3° for the 25 and 13 July. The two WorldView scenes were acquired with in-track viewing angles of −28° and 5.6° and cross-track viewing angles of 12.5° and 14.5°, resulting in a mean GSD of 0.69 m and 0.52m. The triplets or stereo pair were independently processed by using MicMac, which is a free and open-source photogrammetric library [29] (http://micmac.ensg.eu (accessed on 30 June 2022)) to develop 3D reconstruction scenarios. The resulting DSMs have a spatial resolution of 1 m and all include artifacts due to different problems in the source imagery (Figure 2b,d,f).

As easily seen from Figure 2, the three DSMs show false morphologies generated by the presence of meteorological clouds and volcanic degassing. In particular the DSM derived from WorldView-1 (Figure 2f) present an highly impacted region in the north-west portion of the examined area, while the two Pleiades DSMs (Figure 2b,d) display some smaller zones characterized by holes or irregularities in the south-west part. Moreover, the eastern sector, that is the Valle del Bove area, is less defined and detailed in the Pleiades-derived DSMs with respect to the WorldView-1 one.

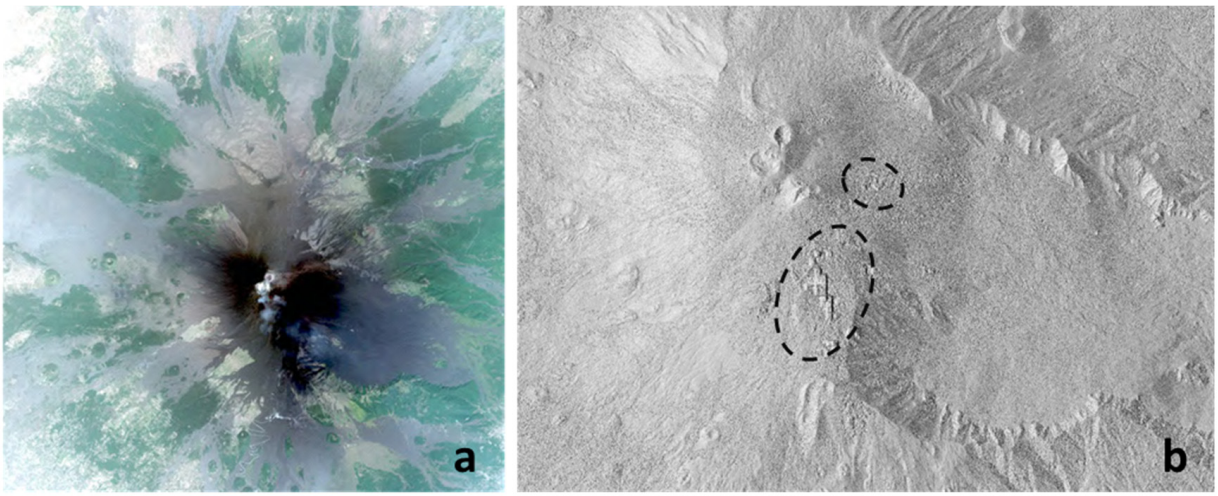

Figure 2. *Cont.*

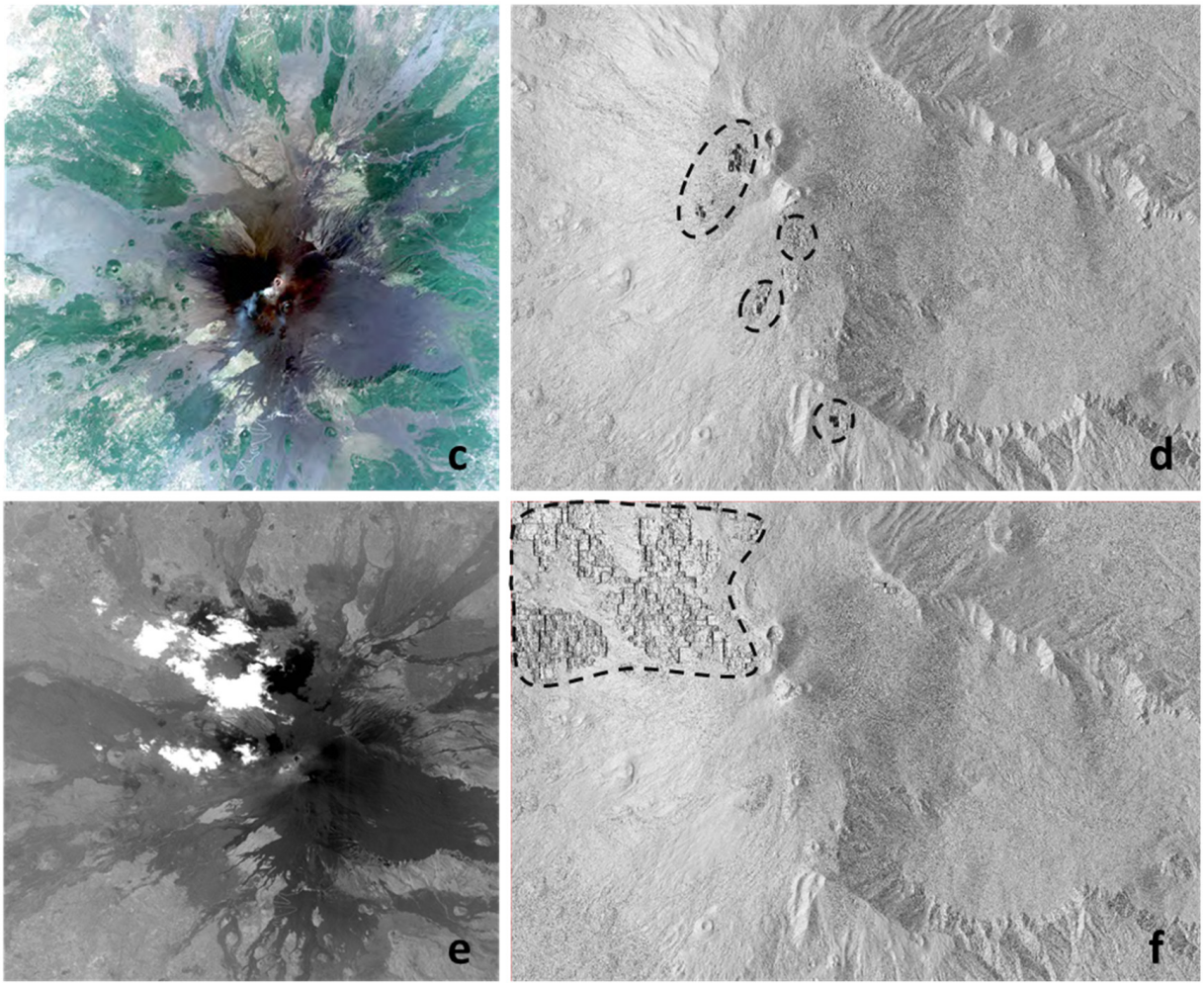

Figure 2. Pleiades images acquired on 13 (**a**) and 25 (**c**) July 2021 with the derived DSMs respectively (**b**,**d**). WorldView-1 scene of 27 July 2021 (**e**) and the derived DSM (**f**), with different false morphologies (dotted black areas).

3. Results

For our case study, we established square patches with sizes of 200 to 1500 m (using a step of 100 m) and computed fourteen DSMs by merging all patches that were selected as the least noisy ones, that is the one with the minimum standard deviation of the Laplacian operator among the three. The fused 1-m DSM was finally obtained by calculating the pixel-per-pixel median of the fourteen DSMs.

The DSM of Mt Etna, obtained from the fusion of three satellite-derived DSMs, has a horizontal resolution of 1 meter and spans an area of ~12 × 8 km, which covers the summit craters and a portion of the south-east flank of the volcano, including the upper part of the Valle del Bove (Figure 3 and electronic supplement 1). The lowest elevation is 1080 m a.s.l., while the highest point of 3347 m is reached on the north rim of the SEC (see also the electronic supplement 1), suggesting a height increase of 60 m in about 6 years [22]. Quality enhancement of the fused DSM is visible to the naked eye, with major improvements in the north-west portion of the summit area (see also the electronic supplement 2), where meteorological clouds affect the WorldView-1 image (Figure 2e,f).

In order to estimate the accuracy of the fused DSM and prove its reliability with respect to the three satellite-derived DSMs, we used 152 GPS Ground Control Points (GPCs), with centimetric vertical accuracy [30], available on Etna volcano (Figure 4a) outside the volcanic deposits emplaced between 2015 and 2021. We measured the elevation difference between each DSM and the GCPs, finding distributions of residuals that peaked to zero (Figure 4b).

The standard deviations of the three satellite-derived DSMs are 3.2 m (Pléiades of 13 July), 3 m (Pléiades of 25 July) and 2.6 m (WorldView-1), while for the fused one, we found a standard deviation of 1.8 m, which gives its vertical accuracy.

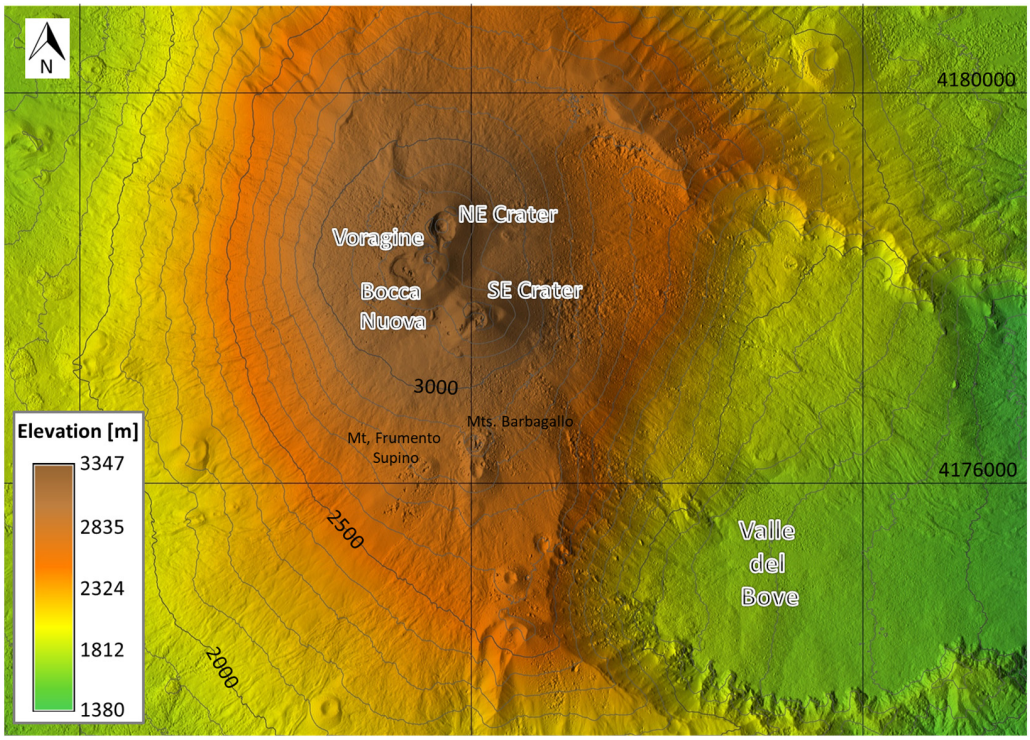

Figure 3. Digital Surface Model (DSM) of Etna volcano obtained by fusing three satellite-derived DSMs (shown in Figure 2b,d,f), updated to July 2021. Voragine (VOR, built in 1945), Bocca Nuova (BN, 1968), North-East Crater (NEC, 1911) and South-East Crater (SEC, 1971) are the present-day summit craters of the volcano. Valle del Bove is a morphological depression on the eastern flank of Etna. A more detailed map is represented as an electronic supplement.

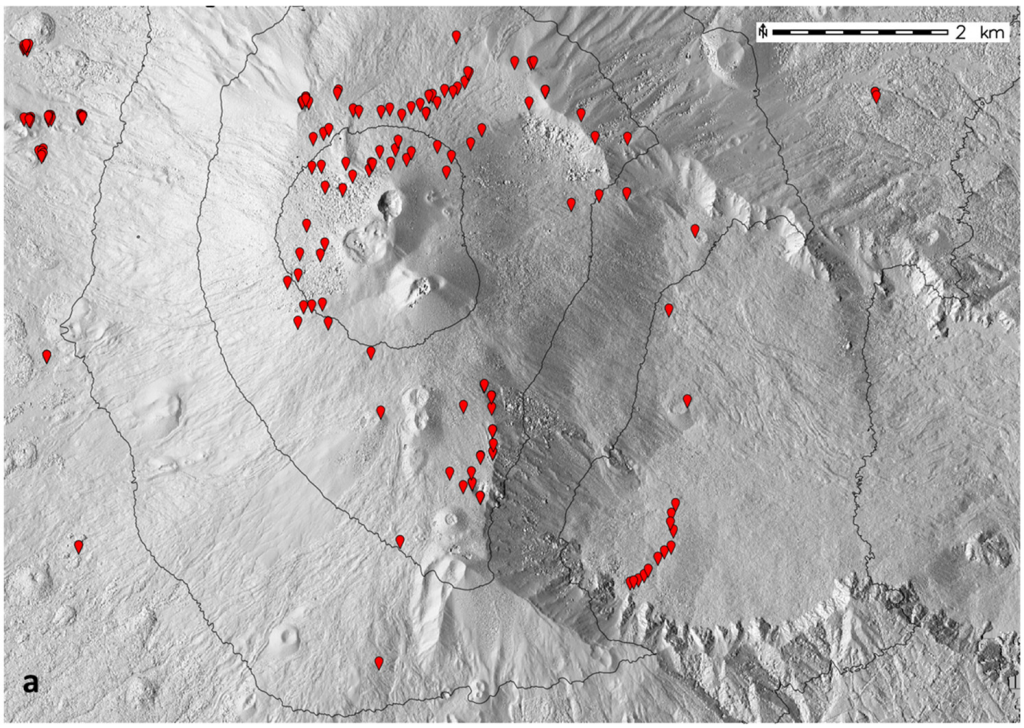

Figure 4. *Cont.*

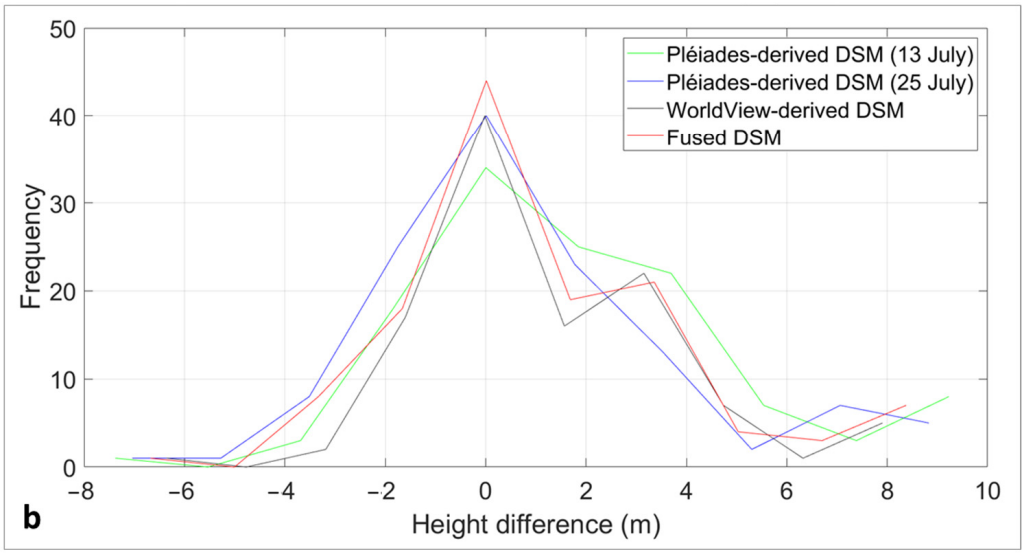

Figure 4. (**a**) Spatial distribution of the GPS Ground Control Points (GCPs, red symbols) used to validate the fused Digital Surface Model (DSM); (**b**) Histogram of the residuals of the three input DSMs and the fused one, all peaking at zero, proving their correct co-registration.

We also estimated the Etna morphological variations occurred since 2016, by performing a comparison with a previous published and validated DSM. Indeed, we computed the difference between our fused 2021 DSM and one obtained by processing a tri-stereo Pléiades 1A imagery acquired on 18 July 2016 (downloadable from https://doi.pangaea.de/10.1594/PANGAEA.899176 (accessed on 15 September 2022)). During 2016-2021, the eruptive activity at Mt Etna was characterized by an intense summit activity with the major episodes occurred from February to April 2017 (6 events), in August 2018 (1 event), between May and July 2019 (3 events), from December 2020 to July 2021 (59 events). A short flank eruption also occurred on Christmas Eve, in December 2018 [28,31,32]. This activity resulted in a multitude of lava flows mainly overlapping in the Valle del Bove area and huge pyroclastic materials accumulated in the SE Crater producing a conspicuous growth and reshaping of the cone.

The volcanic deposits emplaced between 19 July 2016 and 27 July 2021 cover an area of about 9 km^2, with a maximum length of 4.8 km due to the lava flow of the December 2018 flank (Figure 5). The total volume, calculated by integrating the elevation difference over the whole area, amounts to 118.9 $\pm$ 11.6 million cubic meters, with a yearly average volume of 23.8 $\times$ 10^6 m^3/y comparable with the previous studies [3,15]. Of these, 83.6 $\pm$ 11.5 $\times$ 10^6 m^3 are lava flows, while the volume of deposits around the crater area is 35.3 $\pm$ 1.1 $\times$ 10^6 m^3. The average and maximum thicknesses of the lava flows are 10.1 and 20.7 m, respectively. The maximum variation of elevation (120 m) is reached in the south-west rim of the SEC.

In terms of long-term output, 118.9 $\pm$ 11.6 $\times$ 10^6 m^3 of lava erupted in almost 5 years, which results in a time-averaged rate of 0.75 $\pm$ 0.08 m^3 s^{-1}. This estimate falls within the range between 0.6 and 0.9 m^3 s^{-1} that characterizes the high eruption rate phase of Etna beginning in 1971 [33].

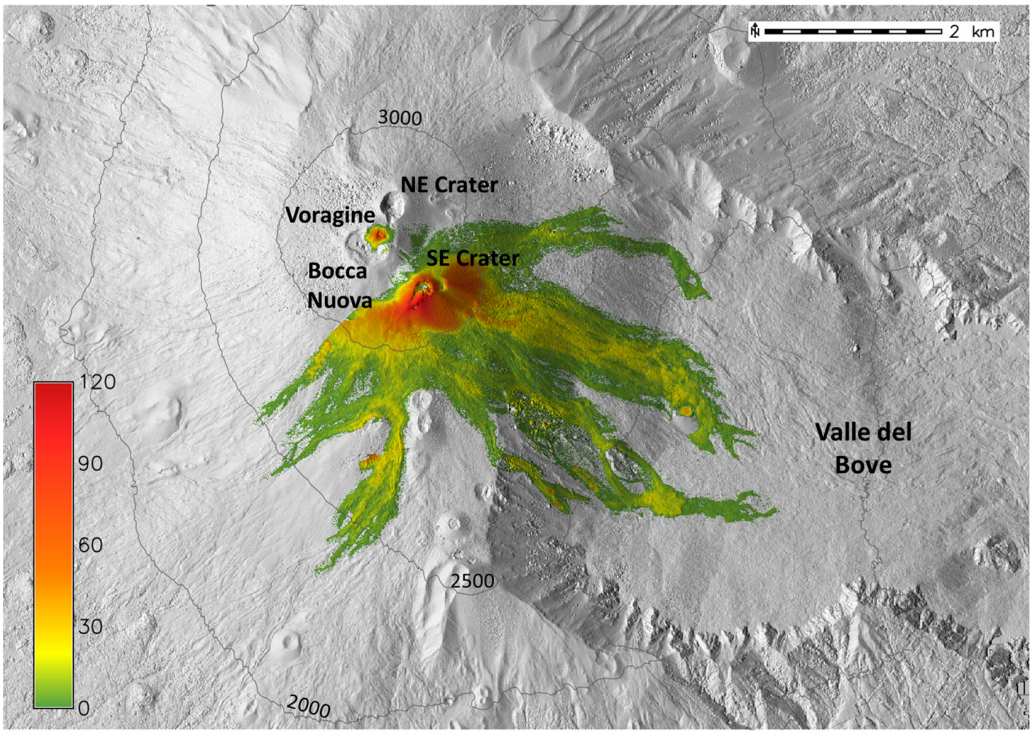

Figure 5. Elevation difference in meters between the 2021 and 2016 Digital Surface Models.

4. Discussion and Conclusions

In this paper, we introduced a novel algorithm for the fusion of DSMs, which is able to automatically remove noise and artifacts in satellite optical images. The algorithm was used to derive the 2021 DSM of Etna's summit area, where relatively large changes occur over short timescales due to the persistent eruptive activity at the summit craters. Three optical images were used in almost the whole area, except inside the area covered by the products emitted during the eruptive event that occurred on 20 July 2021 (INGV Internal Report 30/2021). Indeed, inside this area, the fusion algorithm was applied by considering only the two post-eruptive DSMs.

Our algorithm exhibits excellent performance, providing a detailed elevation dataset even in remote locations, with low running times and no need for post-processing operations. Moreover, unlike most of the algorithms present in the literature, the presented algorithm allows one to merge multiple (more than two) DSMs in a simple way with minimum human interaction, obtaining even more complete and accurate results. Indeed, standard fusion techniques, such as the weighted method, remove those pixels contaminated by clouds and artifacts, but often need a post processing step, such as a smoothing algorithm [19]. Most of the smoothing algorithms introduce further errors to the final products, so avoiding this step represents a great advantage.

Obviously, the accuracy of a satellite-derived DSM depends on different factors, including the resolution of the source images, the methodology used to process the data, and the roughness of the terrain surface. Indeed, it has been demonstrated that the land cover influences the error budget of the derived DSM, with the accuracy over forested areas being lower than over bare land (e.g., [34]). Furthermore, the simultaneous occurrence of various factors such as clouds, volcanic outgassing, morphological instability of slopes and crater rims, snow cover, anthropogenic activities, can further complicate the elaboration of the DSMs.

A downside of our approach is represented by the limited availability of stereo or tristereo archive data and the high cost of on-demand precision data. This could be easily overcome by new satellite missions. As an example, while today, Planetscope data from Cubesat satellites are acquired daily in each point of the Earth's surface at 3.7 m spatial

resolution, allowing one to obtain 7 m spatial resolution DSMs [35], 2080 nanosatellites are planned to be launched from 2022 to the end of 2027, with increasing spatial and spectral resolution. These will guarantee more ground coverage, greater built-in redundancy, and shorter revisit times, available for a much lower price than conventional big satellites [36].

Our procedure has been applied to Etna volcano because it is one of the most active volcanoes in the world, with 10 flank eruptions and several hundred summit eruptions in the last two decades ([25] and references therein). These eruptions cause continuous and consistent morphological changes, especially in the summit area, posing the need for a continuous update, in order to produce accurate mapping and quantification of the volcanic products, as well as for monitoring, forecasting and assessing of volcanic hazards. Indeed, the frequent eruptive summit activity leads to the accumulation of volcanic deposits, especially of unconsolidated pyroclastic material, which can cause instability and collapses of the summit craters' slope and thus produce very fast pyroclastic density currents that can be very dangerous for people and tourists who visit and work in the vicinity of the summit of Etna [37]. This was the case of 10 February 2022 at Mt Etna, when a pyroclastic avalanche occurred from the highest accumulation area of proximal pyroclastic deposits (thickness greater than 100 m) in the south flank of the SEC crater (Figure 5). This kind of event represents the most dangerous hazard linked to the explosive eruptions at Etna's summit, since the pyroclastic density current traveled at more than 100 km/h, covering a distance of ~1.5 km in an area usually frequented by tourists. A near-real-time topographical monitoring, by using the satellite images together with our fusion algorithm, could lead, among other things, to establishing the probability of triggering such dangerous phenomena and, hence, improve the assessment of the associated hazard.

In a wider perspective, the procedure has general validity, as it can be used to derive elevation dataset in all geologic environments prone to frequent and significant morphological changes, even in extreme and remote lands, as long as high-resolution satellite data are available.

Supplementary Materials: The following supporting information can be downloaded at: https://www.mdpi.com/article/10.3390/rs15010198/s1, (1) Detailed map (scale 1:10,000) of the 2021 digital topography of Etna volcano summit. (2) GeoTIFF of the north-west portion of Etna summit area.

Author Contributions: Conceptualization, G.G.; methodology, G.G. and A.C.; validation, M.N.; formal analysis, M.N.; investigation, G.G.; resources, A.C. and G.G.; data curation, A.C. and M.N.; writing—original draft preparation, G.G., A.C. and M.N.; writing—review and editing, G.G., A.C. and M.N.; visualization, A.C. and M.N. All authors have read and agreed to the published version of the manuscript.

Funding: This work was supported by the INGV project Pianeta Dinamico (CUP D53J19000170001) funded by MIUR ("Fondo finalizzato al rilancio degli investimenti delle amministrazioni centrali dello Stato e allo sviluppo del Paese," legge 145/2018), Tema 8—PANACEA. The research was also supported by "TUNE—Effusion rate estimates at Etna and Stromboli: constraints imposed by a variety of satellite remote sensing data" (Bando di Ricerca Libera 2019 of INGV).

Data Availability Statement: Pléiades imagery is available through the Mt Etna supersite initiative see http://geo-gsnl.org/supersites/permanent-supersites/mt-etna-volcano-supersite-new/ (accessed on 15 September 2022). MicMac photogrammetry software is freely available at https://micmac.ensg.eu/index.php/Install (accessed on 30 June 2022). A detailed Map of Mt Etna is provided as Supplementary Material.

Acknowledgments: The authors would like to thank the GNSL Mt Etna Volcano Supersite.

Conflicts of Interest: The authors declare no conflict of interest.

References

1. Grosse, P.; de Vries, B.v.; Euillades, P.A.; Kervyn, M.; Petrinovic, I.A. Systematic morphometric characterization of volcanic edifices using digital elevation models. *Geomorphology* **2012**, *136*, 114–131. [CrossRef]
2. Diefenbach, A.K.; Bull, K.F.; Wessels, R.L.; McGimsey, R.G. Photogrammetric monitoring of lava dome growth during the 2009 eruption of Redoubt Volcano. *J. Volcanol. Geotherm. Res.* **2013**, *259*, 308–316. [CrossRef]
3. Ganci, G.; Cappello, A.; Bilotta, G.; Hérault, A.; Zago, V.; Del Negro, C. Mapping volcanic deposits of the 2011–2015 Etna eruptive events using satellite remote sensing. *Front. Earth Sci.* **2018**, *6*, 83. [CrossRef]
4. Ganci, G.; Cappello, A.; Zago, V.; Bilotta, G.; Hérault, A.; Del Negro, C. 3D Lava flow mapping of the 17–25 May 2016 Etna eruption using tri-stereo optical satellite data. *Ann. Geophys.* **2019**, *62*, VO220. [CrossRef]
5. Ganci, G.; Cappello, A.; Bilotta, G.; Del Negro, C. How the variety of satellite remote sensing data over volcanoes can assist hazard monitoring efforts: The 2011 eruption of Nabro volcano. *Remote Sens. Environ.* **2020**, *236*, 111426. [CrossRef]
6. Heid, T.; Kääb, A. Evaluation of existing image matching methods for deriving glacier surface displacements globally from optical satellite imagery. *Remote Sens. Environ.* **2012**, *118*, 339–355. [CrossRef]
7. Miura, H. Fusion analysis of optical satellite images and digital elevation model for quantifying volume in debris flow disaster. *Remote Sens.* **2019**, *11*, 1096. [CrossRef]
8. Pereira FJ, S.; Costa CA, G.; Foerster, S.; Brosinsky, A.; de Araújo, J.C. Estimation of suspended sediment concentration in an intermittent river using multi-temporal high-resolution satellite imagery. *Int. J. Appl. Earth Obs. Geoinf.* **2019**, *79*, 153–161. [CrossRef]
9. Del Negro, C.; Cappello, A.; Neri, M.; Bilotta, G.; Hérault, A.; Ganci, G. Lava flow hazards at Mount Etna: Constraints imposed by eruptive history and numerical simulations. *Sci. Rep.* **2013**, *3*, 3493. [CrossRef]
10. Del Negro, C.; Cappello, A.; Bilotta, G.; Ganci, G.; Hérault, A.; Zago, V. Living at the edge of an active volcano: Risk from lava flows on Mount Etna. *GSA Bull.* **2019**, *132*, 1615–1625. [CrossRef]
11. Cappello, A.; Bilotta, G.; Ganci, G. Modeling of Geophysical Flows through GPUFLOW. *Appl. Sci.* **2022**, *12*, 4395. [CrossRef]
12. Fu, W.; Ma, J.; Chen, P.; Chen, F. Remote Sensing Satellites for Digital Earth. In *Manual of Digital Earth*; Guo, H., Goodchild, M.F., Annoni, A., Eds.; Springer: Singapore, 2020. [CrossRef]
13. Rogers, S.R.; Manning, I.; Livingstone, W. Comparing the Spatial Accuracy of Digital Surface Models from Four Unoccupied Aerial Systems: Photogrammetry Versus LiDAR. *Remote Sens.* **2020**, *12*, 2806. [CrossRef]
14. Wang, J.; Gong, K.; Balz, T.; Haala, N.; Soergel, U.; Zhang, L.; Liao, M. Radargrammetric DSM Generation by Semi-Global Matching and Evaluation of Penalty Functions. *Remote Sens.* **2022**, *14*, 1778. [CrossRef]
15. Bisson, M.; Spinetti, C.; Andronico, D.; Palaseanu-Lovejoy, M.; Buongiorno, M.F.; Alexandrov, O.; Cecere, T. Ten years of volcanic activity at Mt Etna: High resolution mapping and accurate quantification of the morphological changes by Pleiades and Lidar data. *Int. J. Appl. Earth Obs. Geoinf.* **2021**, *102*, 102369. [CrossRef]
16. Fornaciai, A.; Behncke, B.; Favalli, M.; Neri, M.; Tarquini, S.; Boschi, E. Detecting short-term evolution of Etnean scoria cones: A LIDAR-based approach. *Bull. Volcanol.* **2010**, *72*, 1209–1222. [CrossRef]
17. Mudd, S.M. Topographic data from satellites. *Dev. Earth Surf. Process.* **2020**, *23*, 91–128.
18. Jacobsen, K.; Topan, H. DEM generation with short base length Pleiades triplet, International Archives of the Photogrammetry. *Remote Sens. Spat. Inf. Sci.-ISPRS Arch.* **2015**, *40*, 81–86.
19. Mazzarini, M.; Favalli, M.; Isola, I.; Neri, M.; Pareschi, M.T. Surface roughness of pyroclastic deposits at Mt. Etna by 3D laser scanning. *Ann. Geophys.* **2008**, *51*, 813–822. [CrossRef]
20. Okolie, C.J.; Smit, J.L. A systematic review and meta-analysis of Digital elevation model (DEM) fusion: Pre-processing, methods and applications. *ISPRS J. Photogramm. Remote Sens.* **2022**, *188*, 1–29. [CrossRef]
21. Shean, D.E.; Alexandrov, O.; Moratto, Z.; Smith, B.E.; Joughin, I.R.; Porter, C.C.; Morin, J.P. An automated, open-source pipeline for mass production of digital elevation models (DEMs) from very high-resolution commercial stereo satellite imagery. *ISPRS J. Photogramm. Remote Sens.* **2016**, *116*, 101–117. [CrossRef]
22. Neri, M.; De Maio, M.; Crepaldi, S.; Suozzi, E.; Lavy, M.; Marchionatti, F.; Calvari, S.; Buongiorno, F. Topographic Maps of Mount Etna's Summit Craters, updated to December 2015. *J. Maps* **2017**, *13*, 674–683. [CrossRef]
23. Corsaro, R.A.; Andronico, D.; Behncke, B.; Branca, S.; Caltabiano, T.; Ciancitto, F.; Cristaldi, A.; De Beni, E.; La Spina, A.; Lodato, L.; et al. Monitoring the December 2015 summit eruptions of Mt. Etna (Italy): Implications on eruptive dynamics. *J. Volcanol. Geotherm. Res.* **2017**, *341*, 53–69. [CrossRef]
24. Marchese, F.; Neri, M.; Falconieri, A.; Lacava, T.; Mazzeo, G.; Pergola, N.; Tramutoli, V. The contribution of multi-sensor infrared satellite observations in studying well-monitored volcanoes: The case of May-August 2016 Mt. Etna activity. *Remote Sens.* **2018**, *10*, 1948. [CrossRef]
25. De Beni, E.; Cantarero, M.; Neri, M.; Messina, A. Lava flows of Mt Etna, Italy: The 2019 eruption within the context of the last two decades (1999–2019). *J. Maps* **2021**, *17*, 65–76. [CrossRef]
26. De Novellis, V.; Atzori, S.; De Luca, C.; Manzo, M.; Valerio, E.; Bonano, M.; Cardaci, C.; Castaldo, R.; Di Bucci, D.; Manunta, M.; et al. DInSAR analysis andanalytical modeling of Mount Etna displacements: The December 2018 volcano-tectonic crisis. *Geophys. Res. Lett.* **2019**, *46*, 5817–5827. [CrossRef]

27. Calvari, S.; Bilotta, G.; Bonaccorso, A.; Caltabiano, T.; Cappello, A.; Corradino, C.; Del Negro, C.; Ganci, G.; Neri, M.; Pecora, E.; et al. The VEI 2 Christmas 2018 Etna Eruption: A Small But Intense Eruptive Event or the Starting Phase of a Larger One? *Remote Sens.* **2020**, *12*, 905. [CrossRef]
28. Calvari, S.; Nunnari, G. Comparison between Automated and Manual Detection of Lava Fountains from Fixed Monitoring Thermal Cameras at Etna Volcano, Italy. *Remote Sens.* **2022**, *14*, 2392. [CrossRef]
29. Rupnik, E.; Daakir, M.; Pierrot Deseilligny, M. MicMac—A free, open-source solution for photogrammetry. *Open Geospat. Data Softw. Stand.* **2017**, *2*, 14. [CrossRef]
30. Ganci, G.; Cappello, A.; Bilotta, G.; Corradino, C.; Del Negro, C. Satellite-Based Reconstruction of the Volcanic Deposits during the December 2015 Etna Eruption. *Data* **2019**, *4*, 120. [CrossRef]
31. Cappello, A.; Ganci, G.; Bilotta, G.; Herault, A.; Zago, V.; Del Negro, C. Satellite-driven modeling approach for monitoring lava flow hazards during the 2017 Etna eruption. *Ann. Geophys.* **2019**, *62*, VO227. [CrossRef]
32. Calvari, S.; Biale, E.; Bonaccorso, A.; Cannata, A.; Carleo, L.; Currenti, G.; Di Grazia, G.; Ganci, G.; Iozzia, A.; Pecora, E.; et al. Explosive Paroxysmal Events at Etna Volcano of Different Magnitude and Intensity Explored through a Multidisciplinary Monitoring System. *Remote Sens.* **2022**, *14*, 4006. [CrossRef]
33. Harris, A.J.L.; Steffke, A.; Calvari, S.; Spampinato, L. Thirty years of satellite-derived lava discharge rates at Etna: Implications for steady volumetric output. *J. Geophys. Res.* **2011**, *116*, B08204. [CrossRef]
34. Poon, J.; Fraser, C.S.; Chunsun, Z.; Li, Z.; Gruen, A. Quality assessment of digital surface models generated from IKONOS imagery. *Photogramm. Rec.* **2005**, *20*, 162–171. [CrossRef]
35. Ghuffar, S. DEM Generation from Multi Satellite PlanetScope Imagery. *Remote Sens.* **2018**, *10*, 1462. [CrossRef]
36. Poghosyan, A.; Golkar, A. CubeSat Evolution: Analyzing CubeSat Capabilities for Conducting Science Missions. *Prog. Aerosp. Sci.* **2017**, *88*, 59–83. [CrossRef]
37. Behncke, B.; Calvari, S.; Giammanco, S.; Neri, M.; Pinkerton, H. Pyroclastic density currents resulting from interaction of basaltic magma with hydrothermally altered rock: An example from the 2006 summit eruptions of Mount Etna, Italy. *Bull. Volcanol.* **2008**, *70*, 1249–1268. [CrossRef]